communications earth & environment

Article

https://doi.org/10.1038/s43247-024-01523-3

Synergistic atmosphere-ocean-ice influences have driven the 2023 all-time Antarctic sea-ice record low

Check for updates

Jinfei Wang [1,2], François Massonnet [2], Hugues Goosse [2], Hao Luo[1], Antoine Barthélemy[2] & Qinghua Yang [1]

Antarctic sea ice extent (SIE) reached a new record low in February 2023. Here we examine the evolution of the coupled ocean-atmosphere-sea ice system during the 12 months preceding the record. The impact of preceding conditions is assessed with observations, reanalyses, and output from the regional ocean-sea ice coupled model NEMO3.6-LIM3. We find that the 2022-2023 sea ice annual cycle was characterized by consistently low SIE throughout the year, anomalously rapid sea ice retreat in December 2022, and nearly circumpolar negative SIE anomalies in February 2023. While advection-induced positive air temperature anomalies inhibited the sea ice growth in most regions, strong southerly winds in the Amundsen-Ross Sea caused by an anomalously deep Amundsen Sea Low in spring transported notable volumes of sea ice northward, triggering an unusually active ice-albedo feedback onshore and favoring accelerated melt towards the minimum. This study highlights the impacts of multifactorial processes during the preceding seasons to explain the recent summer sea ice minima.

Antarctic sea ice plays an essential role in the global climate system through its impacts on ocean–atmosphere interactions[1,2], ocean circulation[3,4], ice-shelf stability[5–7], ice-sheet surface mass balance[8,9], and ecosystems[10,11]. The current state of Antarctic sea ice characterized by frequent record-low sea ice extents (SIE) since 2016, after a slight long-term increase (1979–2014), has been gaining a lot of attention[12,13]. On 21 February 2023, SIE reached a new summer minimum of 1.79 million km^2[14], 6.8% lower than the 2022 minimum and 38% lower than the climatology (1981–2010). Negative SIE anomalies have remained throughout the advance season in 2023 and led to the lowest winter maximum ever observed (16.98 million km^2) on 7 September 2023[15]. To better understand the dominant mechanisms behind the recent extremes, it is necessary to examine and compare each case individually since both similarities and differences exist among them[13,16].

Previous studies on the exceptional sea ice melt during the austral spring and summer 2016–2017 have identified several key drivers susceptible to produce low SIE conditions. These drivers include anomalous atmospheric meridional heat advection associated with a positive zonal wavenumber-3 (ZW3) pattern since August, a deepened Amundsen Sea Low (ASL) in September, a near-record negative Southern Annular Mode (SAM) in November[17–19] and anomalous subsurface ocean warming[20–22]. Those local anomalies have themselves been connected to remote potential drivers like the El Niño–Southern Oscillation (ENSO)[17], the Indian Ocean Dipole (IOD)[23], stratospheric circulation anomalies[23], and decadal sea surface temperature (SST) variability in the tropics[24,25]. In contrast, the 2022 and 2023 summer minima appeared in the context of a positive SAM but were also impacted by an anomalously warm state of the subsurface ocean[13]. The lagged impact of a deepened ASL on summer sea ice through enhanced sea ice export and ice-albedo feedback has been suggested to play an important role in this case[26–28]. Studies have already suggested the possible causes of the 2023 summer minimum, which occurred at a time of a very strong positive SAM and after three La Niña years[13,14]. Further investigation is still necessary to determine the specific conditions leading to this minimum and, by this, to better understand the different processes potentially controlling Antarctic sea ice minima.

In this study, we conducted a year-round (March 2022–February 2023) analysis and investigated the link between the summer 2023 minimum and the conditions during the preceding months using satellite observations, atmospheric reanalyses, and a Pan-Antarctic Regional OCEan-sea ice coupled model (PAROCE; see the "Methods" section, Supplementary Figs. 1–3). By conducting an analysis of these datasets, we are able to propose a consistent story that explains how the summer 2023 SIE record developed owing to the atmospheric, oceanic, and sea ice processes that operated over the 12 months before the record. Specifically, we demonstrate how the deepened ASL in the preceding spring triggered the positive ice-albedo feedback and resulted in the summer sea ice loss in the Amundsen–Ross Sea.

[1]School of Atmospheric Sciences, Sun Yat-sen University and Southern Marine Science and Engineering Guangdong Laboratory (Zhuhai), Zhuhai, China. [2]Earth and Climate Center, Earth and Life Institute, Université catholique de Louvain, Louvain-la-Neuve, Belgium. e-mail: yangqh25@mail.sysu.edu.cn

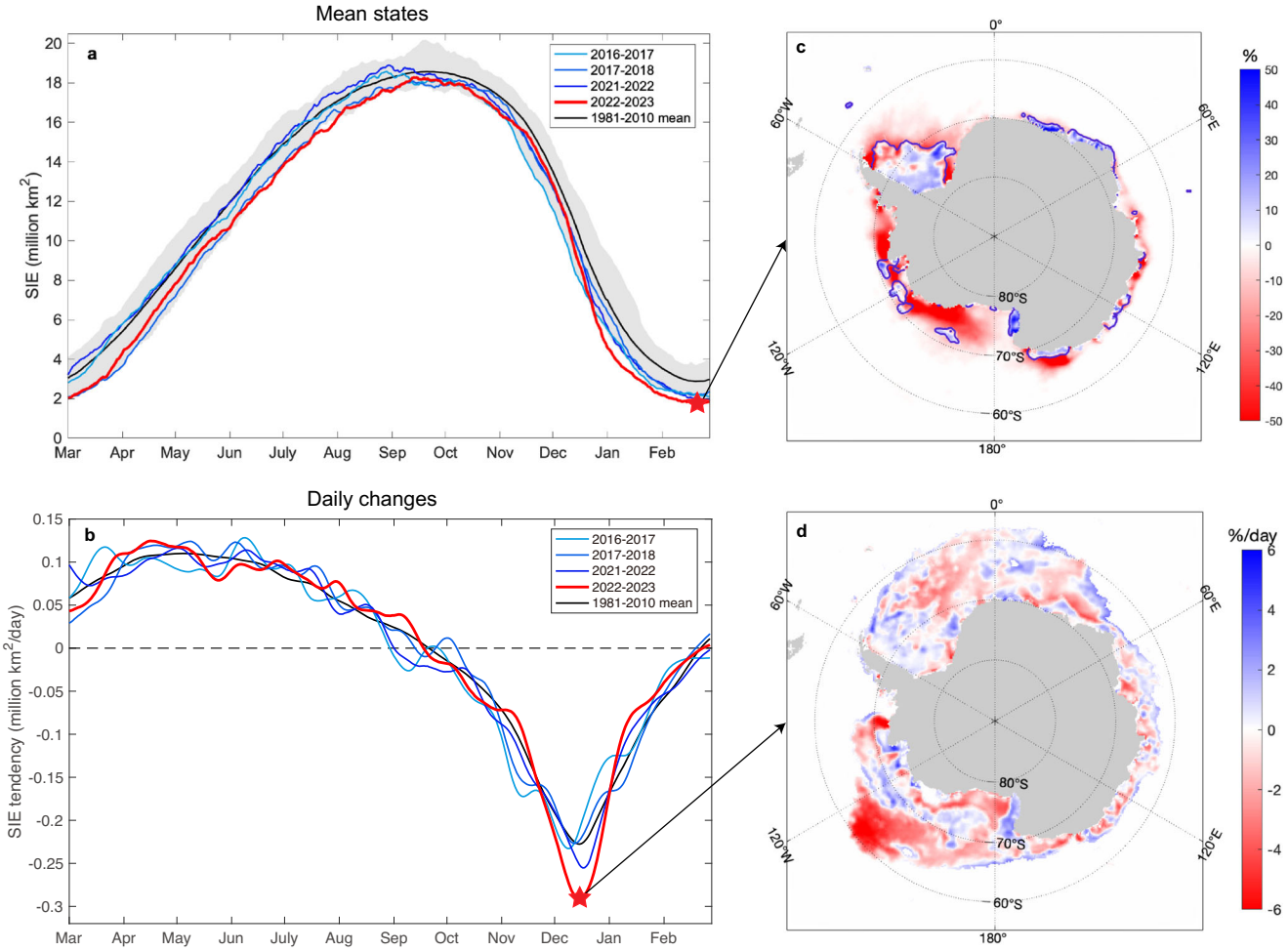

Fig. 1 | Mean states and daily changes of Antarctic SIE annual cycle across multiple extreme years. Observed **a** time series of Antarctic SIE (million km^2) from 1 March to 28 February during 2016–2017, 2017–2018, 2021–2022, 2022–2023, and climatological average (1981–2010) with ranges between daily maximums and minimums during 1979–2022 (shaded). **b** SIE tendency (million km^2 day^{-1}) calculated by central difference for each day from 1 March to 28 February during 2016–2017, 2017–2018, 2021–2022, 2022–2023, and climatology (1981–2010). Sea ice tendency is smoothed by a Gaussian filter. Zero line is indicated by a black dotted line. **c** sea ice concentration (SIC) anomalies (shaded) and sea ice edge (contour) on 21 February 2023. **d** monthly average SIC tendency anomaly in December 2022.

Results

Characteristics of 2022–2023 annual cycle

We start our analysis by characterizing the development of SIE from March 2022 to February 2023 and by placing it in the broader historical context. Figure 1a displays the evolution of observed SIE from March 2022 to February 2023 and compares it with the corresponding observations for 2016–2017 and 2021–2022 (i.e., the two lowest years on record before the event under study), 2017–2018 (i.e., the year following the 2016–2017 summer minimum), as well as the climatological average (1981–2010). We find that the 2023 record results from the combination of two characteristics. First, a consistently lower-than-average SIE prevailed during the whole ice growth season, which found its origin as early as February 2022 (i.e., the previous record), suggesting a strong role for preconditioning. Second, sea ice retreat rates (measured as day-to-day changes in sea ice extent; Fig. 1b) were unusually high in December 2022, reaching the absolute maximum for all the investigated years. This rapid retreat further accelerated sea ice loss towards the summer minimum. It is also worth noting that the 2022–2023 sea ice started to retreat at a normal timing in September (Fig. 1a, b), unlike the earlier retreat during the former two records lows[12,29].

The SIE is a limited indicator of changes as it neglects spatial aspects. A look at the spatial expression of the anomalies discussed above can further direct the search for the mechanisms underlying these changes. On 21 February, when the SIE reached its minimum value, sea ice concentration (SIC) anomalies displayed a nearly circumpolar pattern except in the western Indian Ocean (Fig. 1c), while sea ice anomalies were more regional in the former minimum events[16]. The negative SIC anomalies in 2023 are particularly evident in the Amundsen, Bellingshausen and Ross Seas regions. A spatial look at the sea ice retreat rate anomalies in December (Fig. 1d) reveals that the intense decrease in SIE in December is dominated by strong SIC changes in the north-eastern Ross Sea.

Based on these observations, the 2023 summer SIE minimum can be characterized as (1) having inherited low SIE conditions from the previous summer (2022) and persisted throughout the year, (2) having resulted from rapid late-spring/early-summer retreat rates, which mostly operated in the outer ice pack of the Amundsen–Ross Sea where sea ice normally survives into the summer, and (3) having displayed consistent reductions in other sectors where summer sea ice is climatologically extensive. One exception is the western Indian sector, but the contribution of this sector to the total SIE is negligible (5% for the SIE climatological average)[30].

Recent studies pointed out that subsurface warming played a decisive role in causing more frequent sea ice extremes[13,22]. A potential regime shift to a persistent low-extent sea ice state was also suggested. To explore if the subsurface warming has had an effect on the 2023 summer minimum, we inspected the upper-ocean temperature anomalies in different regions derived from the PAROCE simulation during 2022–2023 (Supplementary

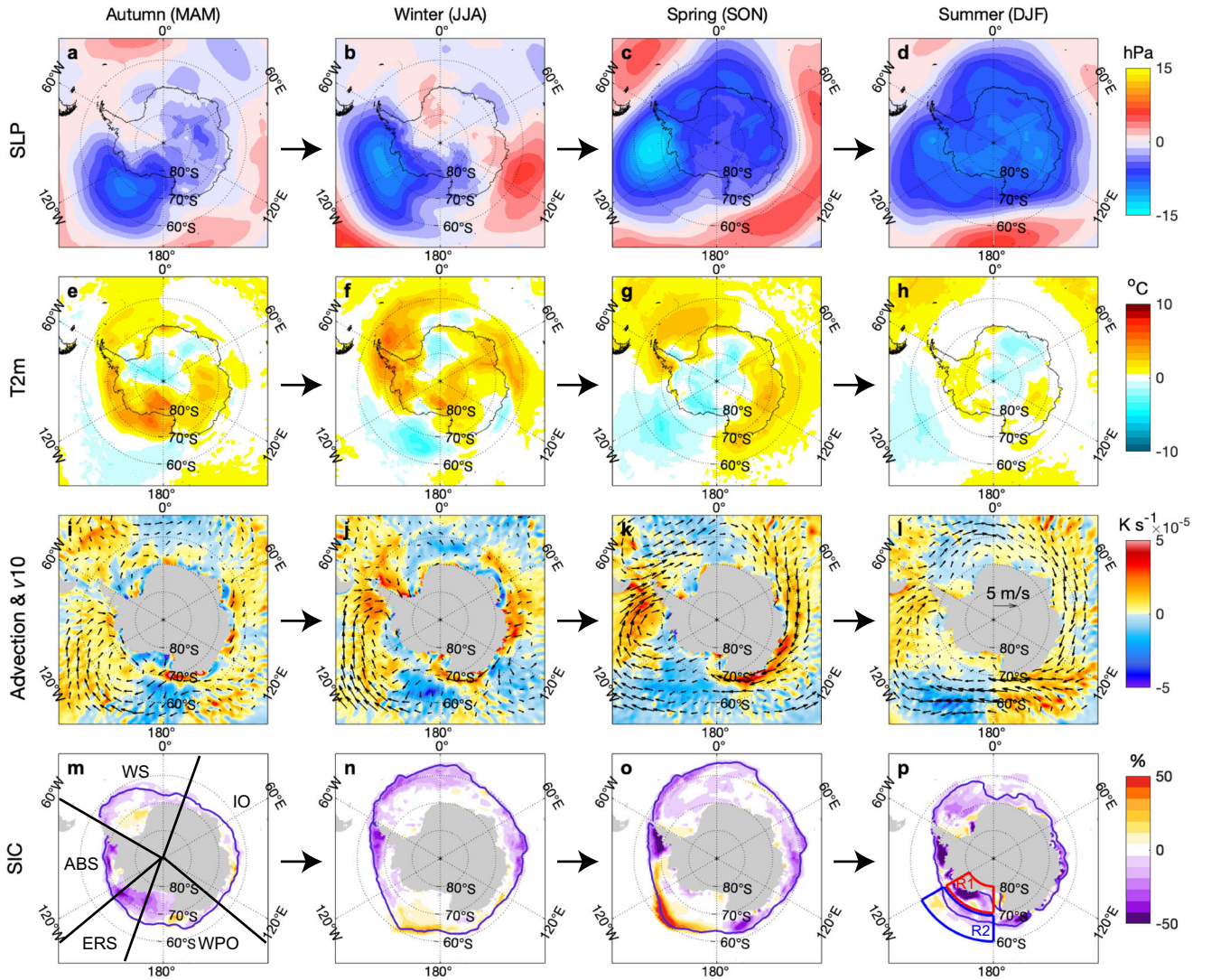

Fig. 2 | Seasonal evolution of atmospheric and sea ice anomalies from March 2022 to February 2023. Anomalies of **a**–**d** SLP, **e**–**h** 2-m air temperature, **i**–**l** temperature advection and 10-m wind, **m**–**p** SIC in autumn (MAM), winter (JJA), spring (SON), summer (DJF) during 2022–2023. Contours **m**–**p** represent climatological (1981–2010) sea ice edge for each season. The Southern Ocean (SO) is divided into WS (Weddell Sea, 60°W–20°E), IO (Indian Ocean, 20–130°E), WPO (Western Pacific Ocean, 130°E–160°W), ERS (Eastern Ross Sea, 130–160°W), and ABS (Amundsen–Bellingshausen Sea, 60–130°W). The red (70–80S, 120–180W, named R1) and blue (60–70S, 120–180W, named R2) box areas (**p**) are used for the sea ice thickness (SIT) budget analysis of the Amundsen–Ross Sea region.

Fig. 4). We find that warmer subsurface ocean conditions have prevailed in all basins of the Southern Ocean in the first 100 m of the ocean, except in the Amundsen and Bellingshausen Seas in summer. The warming was particularly prominent in the Indian and Pacific sectors. We note that the oceanic warming is not specifically high in the eastern Ross Sea, which indicates the potential impacts of other processes on the extreme sea ice melt there. From a long-term perspective (Supplementary Fig. 5), it appears that remarkable warming has also been initiated in these sectors since 2019. A warmer ocean state can favor the basal and lateral melting or hinder the basal growth in such an event, as the basal melt is a dominant source for sea ice melting in the Southern Ocean[31,32], but the detailed mechanism of ice–ocean interactions is beyond the scope of this study. In the following, we will focus on the impacts of local atmospheric processes on the sea ice anomalies and especially investigate the cause of the high retreat rates in the eastern Ross Sea.

Local impacts of atmospheric anomalies

Now that we have described the temporal and spatial characteristics of SIE throughout 2022–2023, we can turn our attention to the candidate mechanisms that drove these changes. We examine here the atmospheric variables and SIC anomalies and their potential mutual connections during the four seasons of 2022–2023. Note that the division of the Southern Ocean here (Fig. 2m) is made as to highlight the special feature of the eastern Ross Sea.

In autumn, a slightly deepened ASL was established in the Amundsen–Ross Sea (Fig. 2a) and air temperature was anomalously warm in the eastern Pacific region (ABS + ERS; Fig. 2e). The intraseasonal air temperature changes mainly come from strong heat transport from lower latitudes through warm air advection (Fig. 2i), hindering offshore sea ice growth in the eastern Pacific region. In the coastal region of the Ross Sea, less sea ice and warmer air temperature can be seen, while cold advection started to prevail and led to decreased temperature anomalies at the end of autumn.

During winter, the negative sea level pressure (SLP) anomaly moved eastward to the ABS region (Fig. 2b), causing positive temperature anomalies in the Weddell Sea, Bellingshausen Sea, eastern Indian Ocean (Fig. 2f) with warm advection and negative SIC anomalies there (Fig. 2j, n). In contrast, more sea ice was produced due to cold advection in the Ross Sea, as expected with the typical ASL pattern.

During spring, the SLP anomaly deepened in the Bellingshausen Sea (Fig. 2c), accompanied by strong warm advection in the Bellingshausen Sea and Eastern Antarctic and cold advection in the Ross Sea (Fig. 2k).

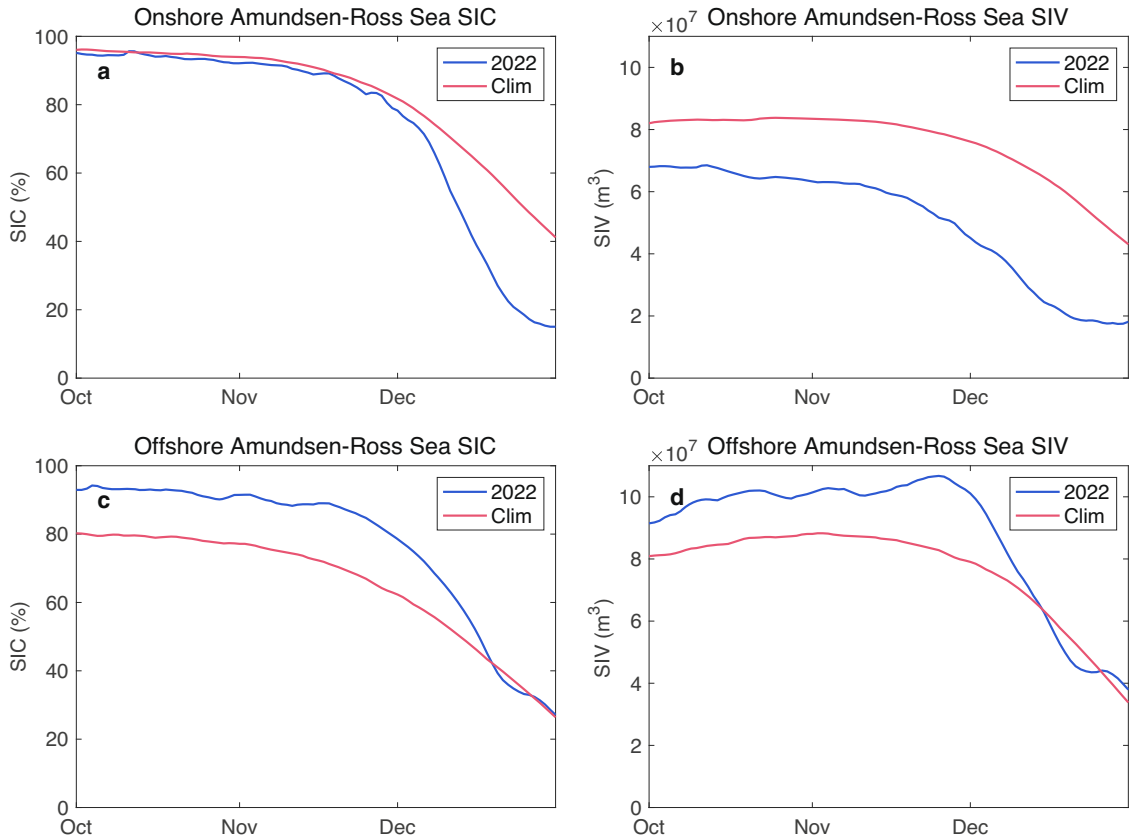

Fig. 3 | Modeled SIC and SIV anomalies in the Amundsen–Ross Sea onshore and offshore regions. Modeled SIC (**a**, **c**) and SIV (**b**, **d**) changes during October–December 2022 and climatology (1981–2010) for the onshore region (70–80°S, 120°W–180) and offshore region (60–70°S, 120°W–180) of Amundsen–Ross Sea region.

Consequently, a SIC dipole (positive anomalies in the Ross Sea and negative ones in the Bellingshausen Sea) appeared, and SIC decreased in the Eastern Antarctic (Fig. 2o). Due to anomalous northerly winds, more ice was transported to the northern Ross Sea and the ice edge was pushed further north by about 2 degrees of latitude till late November (Supplementary Fig. 2a). After that, sea ice edge anomalies retreated abruptly by about 5° of latitude in December. Little ice survived in the Bellingshausen Sea in October after the consistent warm advection pattern that had prevailed.

In summer, a positive annular anomaly (strengthened westerlies/positive SAM) is evident and the regional temperature anomalies were limited. As highlighted by Ferreira et al. [33] and other studies, in response to a positive SAM on short timescale, associated enhanced westerlies will lead to increased equatorward Ekman transport and surface cooling. However, sea ice experienced stronger melting than usual in most regions, and a large open-water area appeared along the coast of Amundsen Sea in December (see the red domain highlighted in Fig. 2p). The observed stronger melting despite the presence of a positive SAM underscores the complex interplay between atmospheric, oceanic, and feedback processes in shaping summer Antarctic sea ice. This apparent inconsistency between the sea ice state and the atmospheric forcing pushed us to elucidate the origins of this coastal open-water area from the aspect of preconditions since the SIE reduction in this region (70–80°S, 120°W–180, named R1 and indicated in Fig. 2p) accounts for 37% of the total reduction in February. A potential mechanism could be that strong winds and strong sea ice transport during the previous months may have led to the emergence of more open water areas, which enhanced the absorption of solar radiation. This strengthened ice-albedo feedback, warmed the surface, accelerated melting rates, and contributed to severe melting in summer, as further demonstrated in the following. In the following section, we test this hypothesis by investigating the related sea ice processes in the Amundsen–Ross Sea.

Impact of spring preconditions in the Amundsen–Ross Sea

Guided by the analysis above, we now focus on the preceding atmospheric impacts on sea ice anomalies in the Amundsen–Ross Sea (120°W–180). We have chosen this broader area to delve into the comprehensive mechanism underlying the extreme reduction of sea ice, particularly in the eastern Ross Sea.

Since the sea ice anomalies happened without significant atmospheric anomalies, we investigate the impacts of preceding sea ice volume (SIV) anomalies by showing the modeled SIC and SIV changes during October–December 2022 and climatology from the PAROCE configuration in the R1 region (Fig. 3a, b). The performance of the model output has been assessed (see the "Methods" section, Supplementary Figs. 1–3) and the model is considered to be sufficiently realistic to reproduce sea ice anomalies in this region. Although SIC showed few anomalies and remained high before December, the SIV has already presented large negative anomalies since the beginning of sea ice growth in 2022 based on the model outputs, indicating that the generally thinner ice along the coast in spring is a potential precondition for the formation of open-water area. The warming subsurface ocean and the low sea ice coverage in summer 2022 may be the causes of those persistent negative SIV anomalies through sea ice–upper ocean interactions. Different from the onshore conditions, sea ice displayed higher SIC than average (Fig. 3c) offshore (60–70°S, 120°W–180, named R2 and indicated in Fig. 2p) and positive anomalies in SIV (Fig. 3d) before December. After that, both SIC and SIV started to decrease. This dipole between negative SIV anomalies close to the coast and positive ones offshore suggests an impact of northward transport from the coastal region to northeastern Ross Sea. A sea ice thickness (SIT) tendency budget analysis is further conducted below with the model outputs to confirm this hypothesis (note that the modeled SIT refers to the grid-cell average thickness and is equal to the SIV divided by the grid cell area).

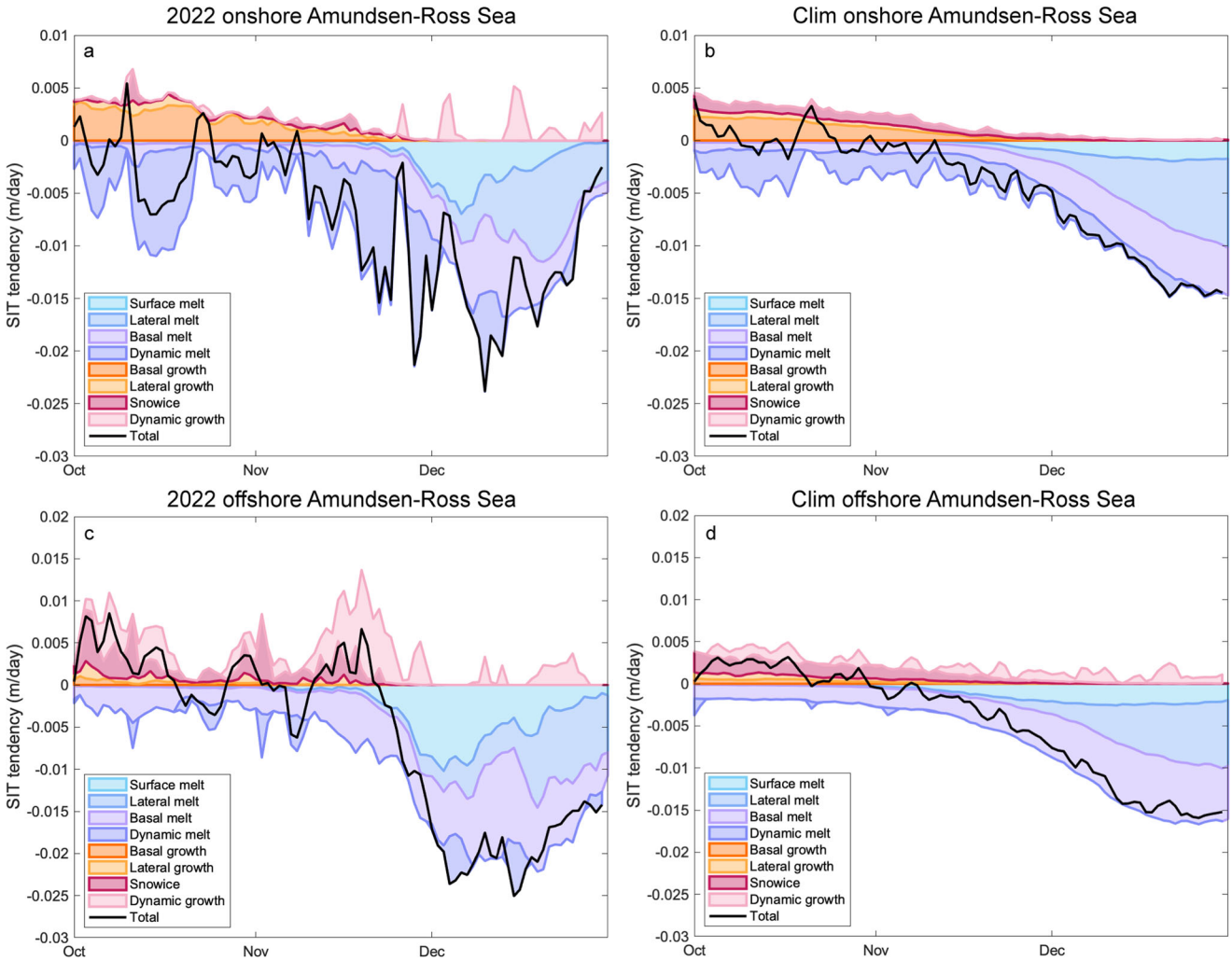

Fig. 4 | SIT tendency budget analysis in the Amundsen–Ross Sea onshore and offshore regions. SIT tendency budgets during **a** October–December 2022 and **b** climatology (1981–2010) for onshore region (70–80°S, 120°W–180) of Amundsen–Ross Sea region based on model outputs, while **c** October–December 2022 and **d** climatology for the offshore region (60–70°S, 120°W–180). The shaded areas depict the cumulative contributions from growth terms (basal growth, lateral growth, growth due to snow-ice formation, growth due to dynamic transportation) and melt terms (surface melt, lateral melt, basal melt, melt due to dynamic transportation) to the overall SIT tendency. The black lines represent the daily SIT changes.

Figure 4 shows the modeled SIT budgets in the R1 and R2 regions during October–December 2022 and climatology and each term has been quantified in Supplementary Tables 1, 2. The daily SIT changes have been divided into growth terms (basal growth, lateral growth, growth due to snow-ice formation, growth due to dynamic transportation) and melt terms (surface melt, lateral melt, basal melt, and melt due to dynamic transportation). In the R1 region, growth terms in 2022 are generally similar to the climatology, except for some transportation-induced growth in December due to anomalous northerly winds (Fig. 2l). However, extreme transportation-induced melt dominated the total SIT tendency from October to late November 2022 (more than twice the climatology), indicating a strong outwards SIV transport. From mid-November to end-December 2022, anomalous melting developed rapidly. This melt was first primarily driven by surface melt (three-fold of climatology), accompanied by growing negative SIC anomalies (Fig. 3a) and thus more open water fraction. From late November onward, oceanic-related melt (basal melt plus lateral melt) took over and accounted for the largest contribution of the total melt (as also observed for the climatology). In late December, the total melt decreased due to little SIV left (Fig. 3b). Correspondingly, in the R2 region, transportation-induced growth, which originates from sea ice transportation, is notably larger from October to November 2022 than climatology. Surface melt is also anomalously large from late-November to mid-December 2022, while oceanic-related melt is also slightly above climatology. Checking the modeled snow depth anomalies over the Amundsen–Ross Sea region (Supplementary Fig. 6), we find that the snow depth presented year-round negative anomalies and a marked drop from September to December, suggesting that surface melt was accompanied by a thinner late-winter/spring snow pack on sea ice.

We also analyze the net surface heat flux anomalies from ERA5 reanalysis and further separate it into long-wave radiation, short-wave radiation, latent heat flux, and sensible heat flux (Supplementary Fig. 7). The net surface heat flux shows increased absorption in the R1 region, dominated by net short-wave radiation flux anomalies. By splitting the net short-wave flux into a downward and an upward component, we can attribute the net surface heat flux anomalies to a less reflective surface, thus implying that the positive ice-albedo feedback[34] controls those net short-wave anomalies.

The deepened ASL in spring has been demonstrated as the potential trigger of positive ice-albedo feedback accompanied by a large sea ice area flux outwards the region[28]. Here, we use the model outputs to calculate the monthly SIV transport outwards the three gates of the R1 region, and to connect them with the changing ASL index with the ice-albedo feedback initiation. Specifically, supplementary Fig. 8 displays the anomalies of the ASL depth, the ASL longitudinal position, the ERA5 meridional winds, the

SIV transport, and the modeled albedo during August–December 2022. The ASL remained deeper than in the climatology throughout the entire winter, spring, and summer seasons. In October, though the depth anomalies were slightly smaller, the ASL was located more eastward than usual, bringing strong southerly winds in the R1 region. Similar ASL conditions lasted until November, resulting in the largest SIV transport anomalies outwards. Consequently, large fractions of open water appeared, surface albedo decreased, and upper-ocean was heated by solar energy, triggering the positive ice-albedo feedback.

Typically, the strengthened ASL is linked to increased warm northerly winds over the Bellingshausen Sea and cold southerly winds over the Ross Sea, generating a dipole-like sea ice response in these regions[35–37]. The contrasting responses of Antarctic sea ice during the 2017, 2022, and 2023 summer minimums, as influenced by ASL variations, underscore the complexity of this relationship and its possible mean-state dependence (Supplementary Fig. 9). In 2016, a record deep ASL in September led to the below-average sea-ice extent in the Amundsen–Bellingshausen and Weddell seas, followed by a weakened ASL (and strong negative SAM) in November associated with warm waters and reduced sea ice in the eastern Ross, Amundsen, and Bellingshausen seas[17,18]. Conversely, during the 2022 and 2023 summer minimums, a deepened ASL in spring brought warm and moist air into the Weddell/Bellingshausen Sea and pushed sea ice northwards in the Amundsen/Ross Sea. The accelerating process of sea ice retreat was attributed to ice-albedo feedback in the Ross Sea region rather than a weakened ASL. We propose two potential reasons for this changed ASL–sea ice relationship. Firstly, as mentioned by previous studies, since the depth and location of the low pressure differ seasonally, the influence of ASL variability on sea ice differs by region and season through changing winds[37,38]. There is also non-stationarity in the link between sea ice and ASL associated with the decreasing zonal symmetry of the circulation in recent years[39]. Thus, we cannot conclude that a deepened ASL will invariably lead to more circumpolar sea ice in summer and the impact of a change in the ASL must be analyzed specifically for each year. Secondly, the warming subsurface ocean and thinning sea ice in recent years may have accelerated sea ice melting in the Amundsen–Ross Sea, both onshore and offshore.

Concluding remarks

The new Antarctic sea ice minimum in the summer of 2023 happened following the last minimum in 2022. The 2022–2023 sea ice evolution featured year-round lower-than-average SIE since March, rapid sea ice retreat in December in the northeastern Ross Sea and a circumpolar melting in summer. In general, negative sea ice anomalies are consistent with advection-induced air temperature anomalies, especially in the Weddell Sea, Bellingshausen Sea and Eastern Antarctic. In the Amundsen–Ross Sea, strong southerly winds driven by ASL transported sea ice along the coast northward, forming a large coastal open-water area and increasing the solar absorption of the upper ocean. As a result, severe surface melting happened, and the ice-albedo feedback amplified the initial change.

For the past few decades, both Global Ice-Ocean Modeling and Assimilation System (GIOMAS) and PAROCE SIT data suggest that Antarctic SIT anomalies mirror the SIE anomalies, with a gradual increase until around 2014 followed by a tendency towards thinner ice since 2016. These changes may be linked to the multiple SIE minimums in recent years; however, more accurate SIT observations are necessary to confirm these trends. According to previous studies in the Arctic[40,41], when SIT approaches a certain threshold (around 0.40–0.50 m), sea ice no longer efficiently insulates the atmosphere and the ocean from one another. Consequently, the atmosphere above such regions is susceptible to more than 2 °C of warming despite ice presence. These changing atmospheric conditions can exert an influence on potential sea ice extent retreat. However, similar investigations have not been conducted in the Southern Ocean, where thin first-year ice predominates. Furthermore, since SIT seems to evolve in sync with SIE from the datasets mentioned above, it is hard to tell if there is a causal relationship between SIT and SIE, or if they are both responding to some external forcing. Hence, detailed research efforts are needed in the future to elucidate these complex dynamics.

The recurrent low summer sea ice minimums in recent years, as well as the exceptionally low winter sea ice maximum in 2023, pose a direct threat to coastal areas. The potential implications encompass coastal erosion, reduced ice-shelf stability, and disruptions to ecosystems. Consecutive observations and improved model performances are imperative to understand the multiscale variabilities inherent in the evolving state of Antarctic sea ice.

Methods

Observations

We used the National Snow and Ice Data Center (NSIDC) daily 25-km gridded SIC products (NSIDC-0051)[42] from 1979 to 2022, while near-real-time products (NSIDC-0081)[43] are used since January 2023. The SIC data is based on passive microwave measurements from the Nimbus-7 SMMR and DMSP SSM/I-SSMIS instruments that are processed with the NASA Team algorithm. We also use the daily NSIDC sea ice index providing consistently processed sea ice extent since 1979, in order to compare the annual cycles among different events.

Reanalyses

Monthly mean SLP, 2-m air temperature, 10-m wind, 1000-hPa air temperature and wind, surface heat fluxes (short-wave radiative flux, long-wave radiative flux, sensible heat flux, latent heat flux) over the period 1979–2023 are obtained from the ERA5 reanalysis[44]. Temperature advection at 1000 hPa is calculated as $-\vec{v}\cdot\nabla T$ with $\vec{v}$ and T being the 1000-hPa horizontal winds and air temperature, respectively. All these variables are available on a grid of 0.25° × 0.25° resolution and have been widely used in Antarctic studies[45–47]. We use 1981–2010 climatology as a baseline to calculate the monthly anomalies following the NSIDC standard. In addition, the GIOMAS SIT reanalyses are used for model validation, consisting of a global Parallel Ocean and Sea Ice Model (POIM)[46] with data assimilation capabilities. GIOMAS data are available from 1979 to the present with a monthly temporal resolution.

Amundsen Sea low (ASL) indices

We use ASL indices[48] to quantify the ASL changes and connect them with sea ice changes. The ASL depth and position are defined as the minimum pressure and its longitude within the ASL sector (170°–298°E, 60–80°S), respectively. ASL indices are derived from monthly ERA5 reanalysis data surface pressure fields.

Models output

A Pan-Antarctic Regional OCEan-sea ice coupled model (PAROCE) integration is used to investigate the SIT budget in the Amundsen–Ross Sea, as SIT measurements from satellite altimetry are still prone to large uncertainties[49,50]. The PAROCE configuration is based on the NEMO3.6 ocean model[51] coupled with the LIM3.6 sea ice model[52,53]. The configuration covers the Southern Ocean south of 30°S. This model is run at a horizontal resolution close to 1/4° (decreasing from 24 km at the 30°S boundary to 14 km at 60°S) and features 75 vertical levels (increasing from 1 m at the surface to about 200 m at depth). The model and configuration have been fully described, evaluated[54], and applied to a recent Antarctic sea ice study[16]. In this study, the model is driven by ERA5 atmospheric reanalysis over the Southern Ocean domain from January 1980 to February 2023 and is forced by the ORAS5 oceanic reanalysis[55] at the ocean boundaries.

Before the SIT budget analysis is conducted from the model output, the model performance has been evaluated. The correlation coefficients between standardized SIE anomalies of NSIDC observations and model output in the Amundsen–Ross Sea region (120°W–180) are significantly high in autumn, winter and spring, showing a high consistency for the long-term changes (Supplementary Fig. 1a–d), while the summer season shows lower correlation. The good agreement between the PAROCE simulation and observations during winter and spring enhances the robustness of our

analysis of the role of preconditioning. Despite the relatively lower (but still statistically significant) correlation in summer for the circumpolar region, the modeled SIC anomalies in the coastal Amundsen–Ross Sea exhibit a high correlation with observations (Supplementary Fig. 1e–g). Besides, the positive anomalies of the sea ice edge (defined as grid cells where SIC is between 14% and 16%) in the eastern Ross Sea (130–160°W) in October and the following abrupt decline in November (~7° retreat in observations and ~9° retreat in model) are captured by the PAROCE simulation (Supplementary Fig. 2b). As we will see, the Amundsen–Ross Sea region (120°W–180) are key area to look at if we want to understand the 2023 summer minimum. The modeled SIC and SIT distributions in this region in December are compared against SIC observations (NSIDC) and SIT reanalysis (GIOMAS), which is widely used in the Antarctic sea ice research (Supplementary Fig. 3)[56,57]. The regional average SIC (SIT) anomalies of model outputs and NSIDC (GIOMAS) are −25.3% (−0.6 m) and −13.7% (−0.4 m), respectively. Generally, the PAROCE simulation in the Amundsen–Ross Sea can capture the main features from observations and is thus useful for the SIT budget analysis, albeit showing model biases in summer. Overall, we acknowledge that the model is not perfect, but it is adequate to explore our scientific question.

Sea ice volume flux

Modeled monthly SIC, SIT and sea ice drift (SID) are used to calculate the sea ice volume flux outwards the coastal Amundsen–Ross Sea region (70–80°S, 120°W–180, named R1 and indicated in Fig. 2p). The values on the original grids are interpolated on the boundaries of that region at regular intervals based on horizontal resolutions in the model. The sea ice volume flux across the three gates enclosing the R1 region is calculated as

$$flux = \sum_{i=1}^{n} SIC_i \, SIT_i \, SID_i \, \Delta L$$

where SIC_i, SIT_i and SID_i denote the SIC, SIT and SID at each grid point; n denotes the number of intervals along the three gates; ΔL denotes the length of each interval.

Data availability

NSIDC sea ice concentration data are available at https://nsidc.org/data/nsidc-0051/versions/2 with near-real-time data at https://nsidc.org/data/nsidc-0081/versions/2. ERA5 reanalysis data are available at https://www.ecmwf.int/en/forecasts/dataset/ecmwf-reanalysis-v5. The ASL index is accessible at https://scotthosking.com/asl_index. The NEMO3.6 version is available from https://forge.ipsl.jussieu.fr/nemo/browser/branches/UKMO. The GIOMAS SIT reanalysis data are available at http://psc.apl.washington.edu/zhang/Global_seaice/data.html.

Code availability

The scripts used to produce the figures in this paper are archived in Zenodo (https://doi.org/10.5281/zenodo.10879133).

Received: 21 December 2023; Accepted: 19 June 2024;
Published online: 03 August 2024

References

1. Søren, R. et al. Sea ice contribution to the air–sea CO_2 exchange in the Arctic and Southern Oceans. *Tellus B* **63**, 823–830 (2011).
2. Gupta, M., Marshall, J., Song, H., Campin, J.-M. & Meneghello, G. Sea-ice melt driven by ice-ocean stresses on the mesoscale. *J. Geophys. Res.: Oceans* **125**, e2020JC016404 (2020).
3. Li, Q. et al. Abyssal ocean overturning slowdown and warming driven by Antarctic meltwater. *Nature* **615**, 841–847 (2023).
4. Zhou, S. et al. Slowdown of Antarctic bottom water export driven by climatic wind and sea-ice changes. *Nat. Clim. Change* **13**, 701–709 (2023).
5. Massom, R. A. et al. Antarctic ice shelf disintegration triggered by sea ice loss and ocean swell. *Nature* **558**, 383–389 (2018).
6. Teder, N. J., Bennetts, L. G., Reid, P. A. & Massom, R. A. Sea ice-free corridors for large swell to reach Antarctic ice shelves. *Environ. Res. Lett.* **17**, 045026 (2022).
7. Kusahara, K., Tatebe, H., Hajima, T., Saito, F. & Kawamiya, M. Antarctic Sea ice holds the fate of Antarctic ice-shelf basal melting in a warming climate. *J. Clim.* **36**, 713–743 (2023).
8. Trusel, L. D., Kromer, J. D. & Datta, R. T. Atmospheric response to Antarctic Sea-Ice reductions drives ice sheet surface mass balance increases. *J. Clim.* **36**, 6879–6896 (2023).
9. Zhu, Z., Liu, J., Song, M. & Hu, Y. Changes in extreme temperature and precipitation over the southern extratropical continents in response to Antarctic Sea ice loss. *J. Clim.* **36**, 4755–4775 (2023).
10. Lim, S. M., van Dijken, G. L. & Arrigo, K. R. Spatial and interannual variability of Antarctic Sea ice bottom algal habitat, 2004–2019. *J. Geophys. Res.: Oceans* **128**, e2023JC020055 (2023).
11. Swadling, K. M. et al. Biological responses to change in Antarctic sea ice habitats. *Front. Ecol. Evol.* **10**, 1073823 (2023).
12. Raphael, M. N. & Handcock, M. S. A new record minimum for Antarctic sea ice. *Nat. Rev. Earth Environ.* **3**, 215–216 (2022).
13. Purich, A. & Doddridge, E. W. Record low Antarctic sea ice coverage indicates a new sea ice state. *Commun. Earth Environ.* **4**, 314 (2023).
14. Liu, J., Zhu, Z. & Chen, D. Lowest Antarctic Sea ice record broken for the second year in a row. *Ocean–Land–Atmos. Res.* **2**, 0007 (2023).
15. Jena, B. et al. Evolution of Antarctic sea ice ahead of the record low annual maximum extent in September 2023. *Geophys. Res. Lett.* **51**, e2023GL107561 (2024).
16. Mezzina, B., Goosse, H., Klein, F., Barthélemy, A. & Massonnet, F. Atmospheric drivers of Antarctic sea ice extent summer minima. Preprint at https://doi.org/10.5194/tc-2023-45 (2023).
17. Stuecker, M. F., Bitz, C. M. & Armour, K. C. Conditions leading to the unprecedented low Antarctic sea ice extent during the 2016 austral spring season. *Geophys. Res. Lett.* **44**, 9008–9019 (2017).
18. Turner, J. et al. Unprecedented springtime retreat of Antarctic sea ice in 2016. *Geophys. Res. Lett.* **44**, 6868–6875 (2017).
19. Schlosser, E., Haumann, F. A. & Raphael, M. N. Atmospheric influences on the anomalous 2016 Antarctic sea ice decay. *Cryosphere* **12**, 1103–1119 (2018).
20. Campbell, E. C. et al. Antarctic offshore polynyas linked to Southern Hemisphere climate anomalies. *Nature* **570**, 319–325 (2019).
21. Meehl, G. A. et al. Sustained ocean changes contributed to sudden Antarctic sea ice retreat in late 2016. *Nat. Commun.* **10**, 14 (2019).
22. Zhang, L. et al. The relative role of the subsurface Southern Ocean in driving negative Antarctic Sea ice extent anomalies in 2016–2021. *Commun. Earth Environ.* **3**, 302 (2022).
23. Wang, G. et al. Compounding tropical and stratospheric forcing of the record low Antarctic sea-ice in 2016. *Nat. Commun.* **10**, 13 (2019).
24. Li, X., Holland, D. M., Gerber, E. P. & Yoo, C. Impacts of the north and tropical Atlantic Ocean on the Antarctic Peninsula and sea ice. *Nature* **505**, 538–542 (2014).
25. Eayrs, C., Li, X., Raphael, M. N. & Holland, D. M. Rapid decline in Antarctic sea ice in recent years hints at future change. *Nat. Geosci.* **14**, 460–464 (2021).
26. Wang, J. et al. An unprecedented record low Antarctic Sea-ice Eextent during Austral Summer 2022. *Adv. Atmos. Sci.* **39**, 1591–1597 (2022).
27. Turner, J. et al. Record low Antarctic Sea ice cover in February 2022. *Geophys. Res. Lett.* **49**, e2022GL098904 (2022).
28. Wang, S. et al. Contribution of the deepened Amundsen sea low to the record low Antarctic sea ice extent in February 2022. *Environ. Res. Lett.* **18**, 054002 (2023).

29. Handcock, M. S. & Raphael, M. N. Modeling the annual cycle of daily Antarctic sea ice extent. *The Cryosphere* **14**, 2159–2172 (2020).
30. Massonnet, F. et al. SIPN South: six years of coordinated seasonal Antarctic sea ice predictions. *Front. Mar. Sci.* **10**, 1148899 (2023).
31. Singh, H. K. A., Landrum, L., Holland, M. M., Bailey, D. A. & DuVivier, A. K. An overview of Antarctic Sea ice in the Community Earth System Model Version 2, Part I: analysis of the seasonal cycle in the context of sea ice thermodynamics and coupled atmosphere–ocean–ice processes. *J. Adv. Model. Earth Syst.* **13**, e2020MS002143 (2021).
32. Li, S., Huang, G., Li, X., Liu, J. & Fan, G. An assessment of the Antarctic sea ice mass budget simulation in CMIP6 historical experiment. *Front. Earth Sci.* **9**, 649743 (2021).
33. Ferreira, D., Marshall, J., Bitz, C. M., Solomon, S. & Plumb, A. Antarctic Ocean and sea ice response to ozone depletion: a two-time-scale problem. *J. Clim.* **28**, 1206–1226 (2015).
34. Curry, J. A., Schramm, J. L. & Ebert, E. E. Sea ice-albedo climate feedback mechanism. *J. Clim.* **8**, 240–247 (1995).
35. Turner, J. et al. Non-annual atmospheric circulation change induced by stratospheric ozone depletion and its role in the recent increase of Antarctic sea ice extent. *Geophys. Res. Lett.* **36**, L08502 (2009).
36. Hosking, J. S., Orr, A., Marshall, G. J., Turner, J. & Phillips, T. The influence of the Amundsen–Bellingshausen Seas low on the climate of West Antarctica and its representation in coupled climate model simulations. *J. Clim.* **26**, 6633–6648 (2013).
37. Raphael, M. N., Holland, M. M., Landrum, L. & Hobbs, W. R. Links between the Amundsen Sea low and sea ice in the Ross Sea: seasonal and interannual relationships. *Clim. Dyn.* **52**, 2333–2349 (2018).
38. Holland, M. M., Landrum, L., Raphael, M. N. & Kwok, R. The regional, seasonal, and lagged influence of the Amundsen Sea Low on Antarctic sea ice. *Geophys. Res. Lett.* **45**, 234, 227–11. (2018).
39. Schroeter, S., O'Kane, T. J. & Sandery, P. A. Antarctic sea ice regime shift associated with decreasing zonal symmetry in the Southern Annular Mode. *The Cryosphere* **17**, 701–717 (2023).
40. Lang, A., Yang, S. & Kaas, E. Sea ice thickness and recent Arctic warming. *Geophys. Res. Lett.* **44**, 409–418 (2017).
41. Ford, V. L., Frauenfeld, O. W., Nowotarski, C. J. & Bombardi, R. J. Effective sea ice area based on a thickness threshold. *Clim. Dyn.* **56**, 3541–3552 (2021).
42. DiGirolamo, N., Parkinson, C. L., Cavalieri, D. J., Gloersen, P. & Zwally, H. J. *Sea ice Concentrations from Nimbus-7 SMMR and DMSP SSM/I-SSMIS Passive Microwave Data, Version 2* (NASA National Snow and Ice Data Center Distributed Active Archive Center, 2022).
43. Meier, W. N., Stewart, J. S., Wilcox, H., Hardman, M. A. & Scott, D. J. *Near-Real-Time DMSP SSMIS Daily Polar Gridded Sea Ice Concentrations, Version 2* (NASA National Snow and Ice Data Center Distributed Active Archive Center, 2021).
44. Hersbach, H. et al. The ERA5 global reanalysis. *Q. J. R. Meteorol. Soc.* **146**, 1999–2049 (2020).
45. Tetzner, D., Thomas, E. & Allen, C. A validation of ERA5 reanalysis data in the Southern Antarctic Peninsula—Ellsworth Land Region, and its implications for ice core turnerdies. *Geosciences* **9**, 289 (2019).
46. Dong, X. et al. Robustness of the recent global atmospheric reanalyses for Antarctic near-surface wind speed climatology. *J. Clim.* **33**, 4027–4043 (2020).
47. Zhu, J. et al. An assessment of ERA5 reanalysis for Antarctic near-surface air temperature. *Atmosphere* **12**, 217 (2021).
48. Hosking, J. S., Orr, A., Bracegirdle, T. J. & Turner, J. Future circulation changes off West Antarctica: sensitivity of the Amundsen Sea Low to projected anthropogenic forcing. *Geophys. Res. Lett.* **43**, 367–376 (2016).
49. Willatt, R. C., Giles, K. A., Laxon, S. W., Stone-Drake, L. & Worby, A. P. Field investigations of Ku-band radar penetration into snow cover on Antarctic Sea ice. *IEEE Trans. Geosci. Remote Sens.* **48**, 365–372 (2010).
50. Wang, J. et al. A comparison between Envisat and ICESat sea ice thickness in the Southern Ocean. *The Cryosphere* **16**, 4473–4490 (2022).
51. Madec, G. et al. *NEMO Ocean Engine*. Technical report (Insitut Pierre-Simon Laplace, Zenodo, 2017).
52. Vancoppenolle, M. et al. *LIM The Louvain-la-Neuve sea Ice Model*. Technical Report. No. 31 (Note du Pôle de Modélisation de l'Institut Pierre-Simon Laplace, 2012).
53. Rousset, C. et al. The Louvain-La-Neuve sea ice model LIM3.6: global and regional capabilities. *Geosci. Model Dev.* **8**, 2991–3005 (2015).
54. Pelletier, C. et al. PARASO, a circum-Antarctic fully coupled ice-sheet–ocean–sea-ice–atmosphere–land model involving f.ETISh1.7, NEMO3.6, LIM3.6, COSMO5.0 and CLM4.5. *Geosci. Model Dev.* **15**, 553–594 (2022).
55. Zuo, H., Balmaseda, M. A., Tietsche, S., Mogensen, K. & Mayer, M. The ECMWF operational ensemble reanalysis–analysis system for ocean and sea ice: a description of the system and assessment. *Ocean Sci.* **15**, 779–808 (2019).
56. Zhang, J. & Rothrock, D. A. Modeling global sea ice with a thickness and enthalpy distribution model in generalized curvilinear coordinates. *Mon. Weather Rev.* **131**, 845–861 (2003).
57. Liao, S. et al. An evaluation of Antarctic sea-ice thickness from the Global Ice-Ocean Modeling and Assimilation System based on in situ and satellite observations. *The Cryosphere* **16**, 1807–1819 (2022).

Acknowledgements

This study was funded by the National Key R&D Program of China (No. 2022YFE0106300), the National Natural Science Foundation of China (No. 41941009), and the Southern Marine Science and Engineering Guangdong Laboratory (Zhuhai) (Nos. SML2023SP217, SML2023SP219, SML2022SP401). This work has received support from the Belgian Science Policy (BELSPO) project RESIST ("Recent Arctic and Antarctic sea ice lows: same causes, same impacts?").

Author contributions

Qinghua Yang conceived the idea for the study; Jinfei Wang, François Massonnet, Hugues Goosse and Hao Luo performed the calculations and drafted the manuscript; Antoine Barthélemy conducted the experiment; All authors critically discussed the results and contributed to the writing throughout the whole process. Correspondence and requests for materials should be addressed to Qinghua Yang (yangqh25@mail.sysu.edu.cn).

Competing interests

The authors declare no competing interests.

Additional information

Supplementary information The online version contains supplementary material available at https://doi.org/10.1038/s43247-024-01523-3.

Correspondence and requests for materials should be addressed to Qinghua Yang.

Peer review information *Communications Earth & Environment* thanks Ariaan Purich and the other, anonymous, reviewer(s) for their contribution to the peer review of this work. Primary Handling Editors: Keiichiro Hara and Joe Aslin. A peer review file is available.